INTERNATIONAL JOURNAL OF AGRICULTURE & BIOLOGY
ISSN Print: 1560–8530; ISSN Online: 1814–9596
12–290/MFA/201x/14–5–697–704
http://www.fspublishers.org

Full Length Article

Identifying and Mapping Stripe Rust in Winter Wheat using Multi-temporal Airborne Hyperspectral Images

LIN-SHENG HUANG, JIN-LING ZHAO[1]†, DONG-YAN ZHANG, LIN YUAN†, YING-YING DONG† AND JING-CHENG ZHANG†
Key Laboratory of Intelligent Computing & Signal Processing, Ministry of Education, Anhui University, Hefei 230039*, China*
†Beijing Research Center for Information Technology in Agriculture, Beijing 100097, China
[1]Corresponding author's e-mail: aling0123@163.com

ABSTRACT

Plant disease incidence usually has a progress from light infection to severe prevalence. How to dynamically monitor this progress on a tempo-spatial scale has become a pressing issue for farmers and agricultural decision-making. In comparison with traditional field-point based detection and diagnosis, remote sensing techniques have provided cost effective tools for acquiring disease severities and corresponding spatial distribution. The primary objective of this study was to quickly identify and map stripe rust infections in winter wheat using multi-temporal airborne hyperspectral images from a Pushbroom Hyperspectral Imager (PIH) sensor developed by Chinese Academy of Sciences. Three PHI images were acquired from April to May in 2002 during the growing season of winter wheat. After comparatively analyzing the image and spectral properties between normal and diseased points in the PHI images, forty-five field sampling points were used to build a binary linear regression model, with a correlation coefficient (r) of 0.923 and the standard error of 0.108. Additional twenty points were utilized to validate the model and the coefficient of determination (R^2) reached 0.877, which showed that this model was encouraging. When applied the model to the three PHI images, winter wheat fields with different stripe rust infections were identified and mapped with five relative severity levels: normal, light, moderate, serious and very serious. The detection results indicated that stripe rust incidence was progressively severe from jointing to milky stage and it was more severe in the southern part than in the northern part, which were very coincident with the real field survey.

Key Words: Airborne remote sensing; Disease index (DI); Photochemical reflectance index (PRI); Pushbroom hyperspectral imager (PHI); Wheat stripe rust

INTRODUCTION

Wheat (*Triticum aestivum* L.), as one of major consumable food products, is the second leading cereal crop in China. Its yield and quality is significantly associated with food security to a great degree. However, climate fluctuations have created a suitable environment for the incidence of various kinds of pests and diseases (Coakley, 1978; Ahmed *et al*., 2012). Stripe rust (*Biotroph Puccinia striiformis*), caused by *P. striiformis* f. sp. *Tritici*, is one of the most devastating foliar diseases and has caused great yield losses in China's wheat production. Consequently, it is of significance to monitor the infection scope and severity caused by such a disease at a large scale. Nevertheless, conventional disease assessment methods strongly rely on visual observation of optical changes in wheat canopies, which are usually labor-intensive, time-consuming and inaccurate (Parker *et al*., 1995). The developments of remote sensing technology have facilitated the direct detection of foliar diseases under field conditions (West *et al*., 2003). When infected with stripe rust, wheat leaf lesions (pustules) in yellow color are produced and they tend to be grouped in patches. Due to the influence of fungal disease, they show different leaf colors, morphologies and crop densities for diseased wheat canopies in comparison with healthy canopies, which makes it feasible to monitor stripe rust via remote sensing techniques.

During the past dozens of years, there has been much literature produced on detecting crop diseases using different remote sensing data sources and processing techniques. Bravo *et al*. (2003) recognized stripe rust using in-field spectral images taken with a spectrograph mounted in the field in early spring. Moshou *et al*. (2004) performed automatic detection of 'yellow rust' in wheat using reflectance measurements and neural networks. Qin and Zhang (2005) utilized broadband high spatial-resolution airborne data acquisition and registration (ADAR) remote sensing data to detect rice sheath blight by constructing band ratio indices and standard difference indices. Huang *et al*. (2007) detected wheat yellow rust using *in situ* spectral

To cite this paper: Huang, L.S., J.L. Zhao, D.Y. Zhang, L. Yuan, Y.Y. Dong and J.C. Zhang, 2012. Identifying and mapping stripe rust in winter wheat using multi-temporal airborne hyperspectal images. *Int. J. Agric. Biol*., 14: 697–704

reflectance measurements and airborne hyperspectral images. Franke and Menz (2007) executed a spatio-temporal analysis of the infection dynamics (of powdery mildew (*Blumeria graminis*) and leaf rust (*P. recondita*) using three high-resolution remote sensing images, and a decision tree was constructed to classify the levels of disease severity using mixture tuned matched filtering (MTMF) results and the Normalized Difference Vegetation Index (NDVI). Pu *et al*. (2008) used a Compact Airborne Spectrographic Imager-2 (CASI) dataset to detect mortality and vegetation stress associated with a new forest disease. Zhang *et al*. (2011) monitored the incidence and severity of yellow rust by constructing a spectral knowledge base (SKB) of diseased winter wheat plants, which took the airborne images as a medium and linked the disease severity with band reflectance from environment and disaster reduction small satellite images (HJ-CCD) accordingly.

The corresponding studies described above clearly demonstrate the capability and potential of spectral reflectance measurements in quantifying the severities of plant diseases. Three types of remotely sensed data can be generally categorized in identifying and assessing the crop diseases: ground-based, airborne and spaceborne data. However, in general, in-field hyperspectral measurements are usually conducted to monitor crop diseases using portable field spectrometers (Huang & Apan, 2006; Rumpf *et al.*, 2010; Chen *et al.*, 2012). It is sometimes insufficient and inaccurate to represent the incidences of crop diseases of the whole target filed using only some sample points. Conversely, spaceborne remote sensing imagery can acquire high spatial resolution and wide swath images and has the capability to detect the disease, but coarse spectral resolution decreases the finer identification accuracy of diseased plants (Toler *et al*., 1981; Nutter, 1989; Reynolds *et al*., 2012). In comparison with in-field hyperspectral and spaceborne remote sensing data, airborne hyperspectral images can be taken from low-altitude flights, which usually have high spectral and spatial resolutions simultaneously (Zhang *et al*., 2003). In addition, they can be easily obtained according to the practical requirements and are very useful in detecting disease stress for large-scale farming of agricultural crops. Consequently, we shifted the attention to home-made airborne hyperspectral imagery (Pushbroom Hyperspectral Imager, PHI) in China and investigated its performance in monitoring stripe rust infections in winter wheat.

The primary objective of this study was to dynamically monitor the stripe rust incidences on a tempo-spatial scale using multi-temporal airborne PHI images. To extend disease monitoring from dozens of discrete field sampling points to a continuous area, field survey points with different stripe rust infections were firstly used to construct a regression model. Then, the model was applied to PHI images after testing its significance. After identifying the diseased regions, the wheat fields were mapped according to the relative severity levels. The disease incidence and prevalence could be dynamically recorded by analyzing multi-temporal stripe rust infection maps.

MATERIALS AND METHODS

Introduction to experimental site and design: Our experiment was conducted at the National Experimental Station for Precision Agriculture in Xiaotangshan, Changping District, Beijing (116°26.3′ E, 40°10.6′ N), China. This study site has a typical continental, semi-humid, monsoon climate in the temperate zone, with a mean annual temperate of 13°C and a mean annual rainfall of 507.7 mm. At this station, the days are generally cloudless during the winter wheat growing season from April to June, which is a significant prerequisite to acquire excellent airborne remotely sensed images. In addition, the terrain is very flat with a land area of 167 ha and is an ideal venue for experimental designs in precision agriculture and airborne hyperspectral remote sensing.

To generate comparative wheat canopies with different infections, an artificial inoculation was performed in 2002 in accordance with a predefined experimental design. In our study, three wheat fields were planted: a contrast field in northwest direction, an artificially inoculated field in southwest direction and a large-scale field in the eastern direction (Fig. 2a). Additionally, to generate a clear contrast area, a spatial separation was arranged between the normal and artificially inoculated areas. The tested cultivar of winter wheat was 98-100 under the normal water and nutrient treatments, which has moderate resistance to stripe rust. At 5:00 pm on April 1, 2002, stripe rust was artificially inoculated with spore suspensions using spraying method in the target field. After about 20 days, artificially inoculated wheat plants began to show small amounts of stripe rust infection.

Determination of disease severity: Disease severity was determined by visual inspection, which was obtained according to the proportion of a complete leaf covered by stripe rust spores. For each sample plot, 20 wheat plants were randomly selected in an area of 1 m^2 and their disease conditions were respectively surveyed. Then, the plants were grouped into a particular severity level from 9 classifications of disease incidence (x): 0, 1, 10, 20, 30, 45, 60, 80 and 100% covered by stripe rust spores. Here, zero percent showed no incidence and 100% was the most serious incidence. Finally, there were a total of 46 field survey points and their disease indices (DIs) were calculated using the following equation (Li *et al*., 1989).

$$DI(\%) = \frac{\sum(x \times f)}{n \times \sum f} \times 100 \quad (1)$$

Where, n is the highest degree of disease severity observed (in this study, n = 8), f is the total number of leaves of each degree of disease severity.

Derivation of *in situ* hyperspectral measurements: When DIs were inspected, the *in situ* hyperspectral measurements of wheat canopies were taken simultaneously with a field-portable ASD FieldSpec Pro FR 2500 spectrometer in the visible and near infrared (VNIR) and short-wave infrared (SWIR) ranges (350 to 2500 nm). The spectrometer with a 25° field of view (FOV) has a spectral resolution of 3 nm and a sampling interval of 1.4 nm between 350-1000 nm and 2 and 10 nm in the range of 1000-2500 nm. For each sample plot, 10 replicate measurements were carried out at a height of 1.6 m above the ground and the average spectrum was used as the final reflectance. After collecting all the hyperspectral data, some preprocessing tasks must be performed such as spectral curve smoothing, removal of water vapor absorption bands, etc.

Normalized difference vegetation index (NDVI) and photochemical reflectance index (PRI): When wheat is infested with stripe rust, its foliar pigments will be destroyed and foliar physiological activity accordingly decreases. The Normalized Difference Vegetation Index (NDVI), which is very sensitive to the change of canopy structure and biomass, was used to estimate changes in wheat canopies (Rouse *et al*., 1974). Additionally, the Photochemical Reflectance Index (PRI) was also used to monitor the disease. This index was defined at the leaf and canopy levels in the early 1990s to assess the efficiency of a plant's use of absorbed photosynthetic active radiation (APAR) for photosynthesis (LUE) (Gamon *et al*., 1992). They were specifically calculated as follows:

$$\mathrm{NDVI} = \left(\rho_{\mathrm{NIR}} - \rho_{\mathrm{Red}}\right) \Big/ \left(\rho_{\mathrm{NIR}} + \rho_{\mathrm{Red}}\right) \quad (2)$$

$$PRI = \frac{\rho_{531} - \rho_{570}}{\rho_{531} + \rho_{570}} \quad (3)$$

Where, ρ_x corresponds to the reflectance value at specific annotated wavelengths of PHI imagery.

Processing of airborne pushbroom hyperspectral imager (PHI) imagery: PHI was developed by the Shanghai Institute of Technical Physics (SITP), Chinese Academy of Sciences (CAS). The sensor with a field of view of 21°comprises a solid state, area array, silicon CCD device of 780×244 elements, which is capable of acquiring images of 1 m×1 m spatial resolution in the wavelength range of 400–850 nm with a spectral resolution of less than 5 nm (Shao *et al*., 1998; Zhang *et al*., 2000). Three images were acquired in our study during the growing seasons of winter wheat in 2002: jointing stage (April 18), filling stage (May 17) and milky stage (May 31). To perform subsequent analysis accurately, those images were pre-processed for radiometric, spectral and geometric calibration and then they were transformed to reflectance images by field calibration using empirical line method. After checking the image quality of each channel in accordance with the spectral properties of winter wheat, those bands, located in the wavelength range of 400-500 nm and 805-850 nm, were found to be abnormal. Therefore, they were abandoned in this study and the available bands were adopted in the 500-805 nm spectral range.

Linear reversion model and hypothesis testing: Construction of the reversion model is the first step to derive stripe rust infections from multi-temporal PHI images. In comparison with healthy wheat, the stripe rust-infected wheat has usually higher reflectance values in the visible spectrum and lower values in the NIR range (Huang *et al*., 2007; Luo *et al*., 2010). Furthermore, the differences between the visible red and NIR bands are also drastic in accordance with the construction of NDVI (Devadas *et al*., 2009). Therefore, those two bands were selected as the independent variables and the measured DIs were used as the dependent variable to build the binary linear reversion model. To reduce random errors, the average values from 620-718 nm and 770-805 nm were used as the red and NIR bands. It is necessary to test the significance of the model to be better applied in PHI images. F test was used here as follows (Bevington & Robinson, 2003; Downward *et al*., 2007). When the calculated F_{Exp} at a certain significance level (α) is greater than that of $F_\alpha(k, n\text{-}k\text{-}1)$ from F distribution tables, it shows that the significant linear relationship exists between the independent and dependent variables. Otherwise, it will be rejected.

$$F_{Exp} = \frac{\chi_1^2 / k}{\chi_0^2 / (n-k-1)} \quad (4)$$

Where, χ_0^2 represents the statistical χ_1^2 of the better fit; F_{Exp} is denoted as the experimental value of F, which follows the distribution with degrees of freedom of *k*in the numerator and degrees of *n*-*k*-1 in the denominator; *k* is the number of independent variables in the linear regression model; *n* is the total number of samples.

RESULTS

Quantitative analysis of several spectral indicators: To quantitatively compare the differences between normal and diseased wheat canopies, six spectral parameters sensitive to stripe rust infections were selected (Table I). At each growth stage, there were little differences of blue, green and red bands in image textures and color tunings, but the differences were much larger among different stages. As a contrast, the differences were larger whether at the same stage or among three stages for the near-infrared (NIR), NDVI and PRI indicators. At jointing stage, there were just little differences among six parameters owing to early infection, but the differences were furthermore expanded than normal growth status because of the stripe rust infections at the subsequent growth stages. Stripe rust destroyed the pigments and reduced chlorophyll absorption, so the reflectance value of diseased point was higher than that of normal point in the visible spectrum (Blue, Green & Red). Conversely, it was smaller in the near-infrared

Table I: Comparison of some spectral characteristic parameters between normal and diseased points at three growth stages

Spectral parameter	Jointing stage (4/18)			Filling stage (5/17)			Milky stage (5/31)		
	Image	Normal	Diseased	Image	Normal	Diseased	Image	Normal	Diseased
Blue (457.2 nm)	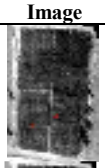	5.55	4.97	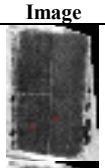	2.98	3.64	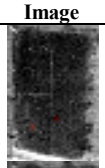	3.32	6.53
Green (570.0 nm)	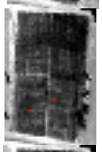	9.03	9.88		6.99	7.83	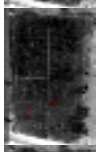	10.57	15.22
Red (682.4 nm)	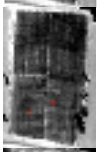	9.47	10.84		2.80	8.45	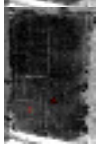	9.86	20.61
NIR (750.1 nm)	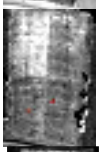	33.37	32.61		54.20	24.87	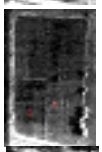	46.54	37.80
NDVI	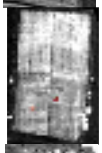	0.561	0.528	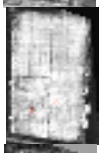	0.909	0.492		0.726	0.294
PRI		-0.088	-0.053		0.011	-0.141		-0.014	-0.155

spectrum, because stripe rust fungus destroyed cell structure and water and reduced the efficiency of wheat's use of APAR and LUE. In comparison with Blue, Green and Red, the values of NIR, NDVI and PRI of diseased wheat decreased in comparison with normal wheat.

Image and spectral characteristics of diseased wheat: Two comparative points were marked on the PHI images of three growth stages and their spectral reflectance curves were also identified (Fig. 2). As shown in those temporal figures, three-band composites were created using near-infrared band (783.5 nm), red band (682.4 nm) and green band (551.0 nm) (as red, green and blue, respectively) to offer best, most intuitive false-color combination. We could find that those land features in red color were primarily green vegetation including wheat canopies and trees. Three images showed different visual effects, especially in the color, as wheat plants progressed through jointing to milky stages. As shown in Fig. 2a, they had similar color tuning by comparing the normal and diseased sampling points. However, there were still some minor differences in their hyperspectral reflectance curves, especially in the near-infrared region. Due to the little influence of stripe rust infection, the reflectance value of diseased point was smaller than that of normal point in the near-infrared region. Conversely, the color tuning was extremely different at filling stage which was the most significant period to form yield (Fig. 2b). It still showed the red color for the normal canopy, while it turned black for the diseased canopy. This phenomenon indicated that stripe rust pathogen had badly affected the wheat canopies, which made them lose the vegetation characteristics of both image and spectrum. Specifically, there were a reflectance peak (centered at 570 nm), an absorption valley (centered at 670 nm) and a high reflection peak in near infrared waveband for the normal canopy, but the green peak disappeared and the red valley was greatly flattened in the visible spectrum and the reflectance obviously decreased in the wavelength range of 715-800 nm for the diseased canopy. At the milky stage, vegetative characteristics had almost lost and it turned black in color tuning on the whole (Fig. 2c). In addition, the spectral curves showed different features for both normal and diseased points. It still showed the spectral characteristics of vegetation for the normal canopy, but it almost showed the spectral characteristics of bare soil and hayfield for the diseased canopy.

Fig. 1: Location of the experimental field in our study

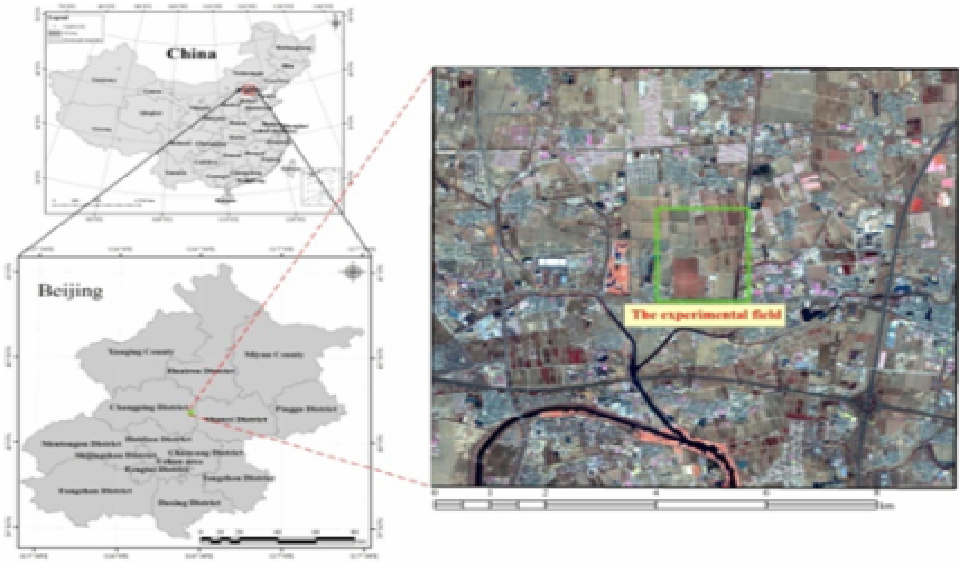

Fig. 2: Comparison of images and spectra of normal and diseased wheat canopies among three growth stages

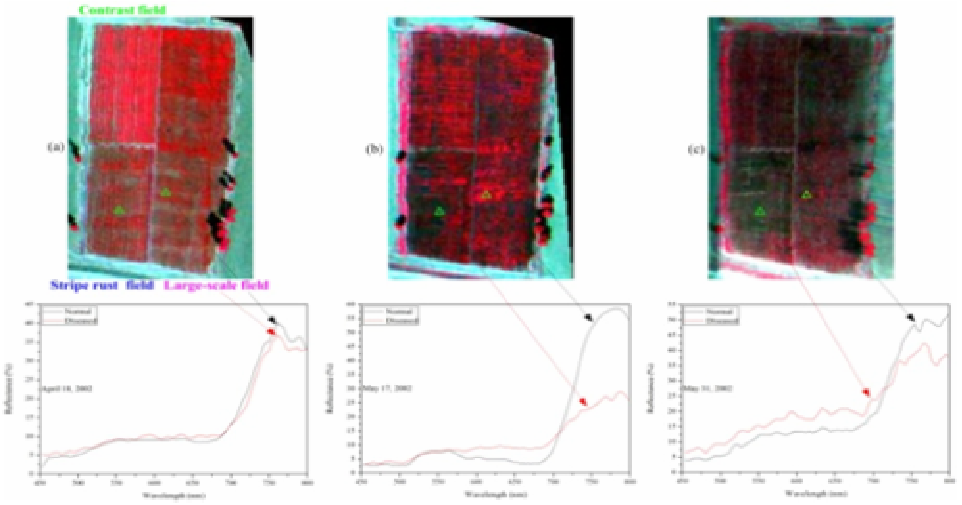

Fig. 3: Validation of the built binary linear regression model using field measurements

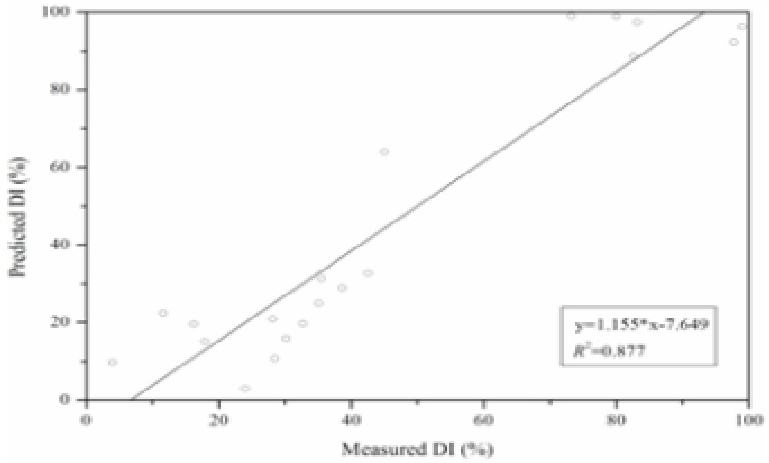

Fig. 4: Three maps of stripe rust infected winter wheat

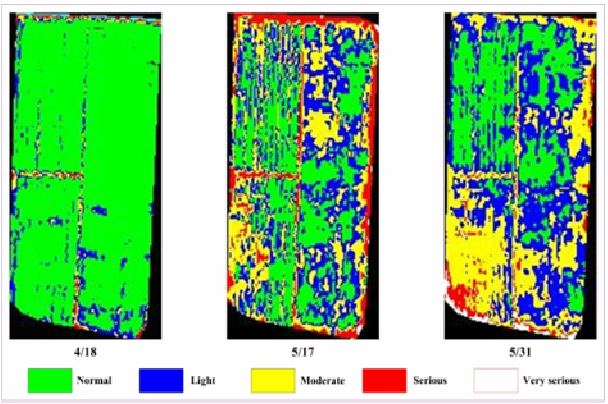

Fig. 5: Typical spectral response properties of green vegetation (after Hoffer, 1978)

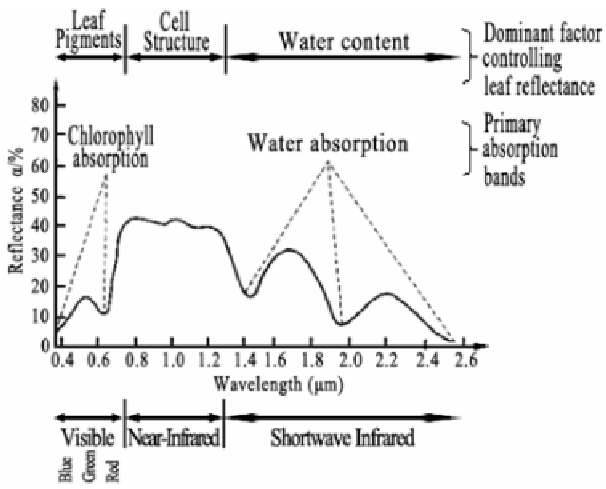

Development and verification of linear regression model: Forty-five field survey points from jointing to filling stages were selected to build a binary linear regression model with a correlation coefficient (r) of 0.923 and standard error of 0.108 (Eq. 4). F-test with a significance level of 0.05 was used for testing the significance of the model. The result showed that the calculated F value of 121.5 was significantly greater than $F_{0.05}$ (2, 42) of 3.23, which indicated that this model was very encouraging. Furthermore, to validate the identification effect of stripe rust, additional twenty points were used to estimate the linear regression between measured and predicted DIs (Fig. 3). The coefficient of determination (R^2) was 0.877, which showed that this model had better estimation efficiency. In the process of acquiring PHI images, it was also inevitable that various factors would affect the reflectance, especially for a certain sensitive band. In our study, average bands of red (621.0-720.1 nm) and near-infrared (768.7-805.7 nm) spectral regions of PHI images were used instead of a particular band.

$$DI = 18.652 * Red - 1.761 * NIR + 7.364 \quad (4)$$

Where, *Red* and *NIR* are respectively the average reflectance values within the wavelength ranges of 620-718 nm and 770-805 nm.

Mapping of stripe rust infections in three PHI images: The developed and tested model was applied to the three PHI images. Relative severity levels were specified according to the DIs: normal (0%-5%), light (5%-25%), moderate (25%-50%), serious (50%-80%) and very serious (80%-100%). As shown in Fig. 4, it was very obvious that the stripe rust infections could be dynamically monitored, especially for the disease severities and spatial distribution. At the jointing stage (4/18), wheat canopies were just infected with stripe rust fungus, so some canopies with light level could be observed. However, serious stripe rust infections could be found in some local regions at the filling stage (5/17). Conversely, more extensive infections occurred at the milky stage, especially in the artificially inoculated wheat field. Concerning the spatial distribution of stripe rust infections, it could be found that disease was more severe in the southern part than in the northern part, especially in the PHI image of 5/31.

DISCUSSION

To accurately identify the diseased wheat from normal wheat using hyperspectral remote sensing dataset, it is necessary to find their spectral differences (Muhammed, 2005).Considering the spectral properties between normal and diseased canopies (Fig. 2), an interesting phenomenon could be found that the reflectance of diseased point was larger than that of normal point in the visible spectrum, while it was smaller in the near-infrared part, which was consistent with the analysis results of other studies (Lorenzen & Jensen, 1989; Malthus, 1993; Carter & Knapp, 2001). For healthy leaves, they have the same optical properties whatever the species are as shown in Fig. 5 (Hoffer, 1978). A green, healthy and vigorously growing plant leaf will generally has typical spectral features: (i) lower reflectance in the visible bands (400-700 nm) due to strong light absorption by various leaf photoactive pigments;(ii) higher reflectance in the NIR spectral domain (700-1300 nm) owing to multiple scattering at the air-cell interfaces in the leaf's internal tissue; and(iii) low reflectance in the short-wave infrared (SWIR, 1300-2500 nm)characterized by the light absorption by the leaf water near 1450, 1950 and 2500 nm (Hoffer, 1978; Huang *et al.*, 2007). In our study, stripe rust infections caused different severities at different growth stages. At the jointing stage, the fungus primarily infected leaves which appeared in rows somewhat linearly along the axis of the leaf. However, infections appeared on the spikes and on the stems of wheat at the filling and milky stages. Finally, the pathogens overcome the host and the fungal urediniospores ruptured through the surface of the leaf, stem, or spike tissues. In addition, as stripe rust destroyed the pigment, chlorophyll and foliar structure of wheat, the nutrient accumulation of

normal growth was shortened and it advanced to mature in advance. Consequently, the leaf area indexes (LAI) and dry matter contents were influenced and the spectral properties were affected (Fig. 2).

In previous studies, different ground-based hyperspectral spectrometers, such as ASD (Analytical Spectral Devices, Inc.) Field Spec Pro spectroradiometers, have been extensively applied in identification and characterization of fungal diseases in wheat (Sharp *et al*., 1985; Chen *et al*., 2012). However, those non-imaging devices usually collect mixed spectral data besides the target feature in a fixed FOV and can only take a point and image it as a line. For instance, the spectra of soil, shadow are always included, when acquiring the diseased wheat canopies using a spectrometer. Consequently, the classification accuracy will be decreased to a great degree. Conversely, imaging spectrometers are being developed with the increasing needs in large-scale precision agriculture. Those devices can obtain image and spectrum with high spatial and spectral resolution of a target feature simultaneously during a scan process. A pixel in the image can correspond to a complete hyperspectral curve in the specific wavelength range. With this capability it is possible to reconstruct the image and spectral characteristics of target features in a heterogeneous FOV, which is capable of satisfying the imaging requirements for more accurate plant disease diagnosis (Clevers, 1999; Jones, 2004). In addition, more complex algorithms will be required to process the images than the non-imaging line data (Moshou *et al*., 2005; Mirik *et al*., 2006). For example, a smoothing processing must be performed to acquire smoothed hyperspectal curves for a pixel. In our study, the adjacent-averaging method with the window of two points was used to smooth the curves due to the influence of background noises.

Concerning the wheat diseases, most of previous studies mainly focus on monitoring and identifying infections at a specific growth stage or a local region (Bravo *et al*., 2003; Nicolas, 2004). Nevertheless, it is more significant to learn about the stripe rust infections on a tempo-spatial scale. The disease severities are generally different at different growth stages during the growing period of winter wheat (Zhang *et al*., 2003). To conduct site-specific fungicide applications, the spatio-temporal dynamics of wheat diseases must be well known. Multi-temporal disease detection provides an effective tool for this dynamic infection process by multi-temporal remote sensing dataset (Franke & Menz, 2007). In our study, three home-made PHI images in China from three key growth stages were acquired to monitor the stripe rust infections in winter wheat. Consequently, the disease severities increased from jointing to milky stage and from north to south. The phenomenon could be interpreted that the inoculation concentrations progressively increased from north to south in the inoculated field. As a result, the diseases spread at a high speed in the wheat plots with higher inoculation concentrations and the diseases were also more severe. The identification results mostly coincided with the field survey condition. However, some misclassifications were also caused in some places, especially in the marginal areas due to the influences of tree shades and bare soil. In the subsequent study, more accurate wheat classification will be required to minimize the influences of backgrounds.

In conclusion, it is always a dynamic infection process for stripe rust fungus in winter wheat. Multi-temporal disease monitoring on a tempo-spatial scale will be prerequisite to implement site- and time-specific fungicide applications. Remote sensing technology provides an effective tool for dynamically detecting the disease incidence. To achieve such a goal, two conditions will be required. On one hand, available remotely sensed images at certain key stages will be important guarantee during the growing season of plant. On the other hand, in-field quasi-synchronizing measurements during the airborne images acquisition are very essential for creating proper ground-based monitoring model. When the significance of the model is tested, it can be only applied into the airborne images. Therefore, based on the *in situ* hyperspectral measurements in our study, it is feasible that multi-temporal airborne images in China are used to dynamically monitor the stripe rust incidence in winter wheat at a relatively large tempo-spatial scale.

Acknowledgement: This work was supported by Postdoctoral Science Foundation of Beijing Academy of Agriculture and Forestry Sciences (2011),China Postdoctoral Science Foundation funded project (20110490317), Beijing Postdoctoral Research Foundation (2012),National Natural Science Foundation of China (41001244,41071276) and the 211 Project of Anhui University (KJQN1121, KJTD007A).

REFERENCES

Ahmed, M., F.U. Hassan, M. Aslam and M.A. Aslam, 2012. Physiological attributes based resilience of wheat to climate change. *Int. J. Agric. Biol*., 14: 407–412

Bevington, P.R. and D.K. Robinson, 2003. *Data Reduction and Error Analysis for the Physical Sciences*,3rd edition. McGraw-Hill, New York, USA

Bravo, C., D. Moshou, J.S. West, H.A. McCartney and H. Ramon, 2003. Early disease detection in wheat fields using spectral reflectance. *Biosyst. Eng*., 84: 137–145

Carter, G.A. and A.K. Knapp, 2001. Leaf optical properties in higher plants: linking spectral characteristics to stress and chlorophyll concentration. *American J. Bot*., 88:677–684

Chen, B., S.K. Li, K.R. Wang and G.Q. Zhou, 2012. Evaluating the severity level of cotton Verticillium using spectral signature analysis. *Int. J. Remote Sens*., 33: 2706–2724

Clevers, J.,1999. The use of imaging spectrometry for agricultural applications. *ISPRS J. Photogramm*., 54: 299–304

Coakley, S.M., 1978. The effect of climate variability on stripe rust of wheat in the Pacific Northwest. *Ecol. Epidemiol*., 68: 207–212

Devadas, R., D.W. Lamb, S. Simpfendorfer and D. Backhouse, 2009. Evaluating ten spectral vegetation indices for identifying rust infectioninindividualwheatleaves.*Precis.Agric*.,10: 459–470

Downward, L., C.H. Booth, W.W. Lukens and F. Bridges, 2007.A variation of the F-test for determining statistical relevance of particular parameters in EXAFS fits.*AIP Conf. Pro*.,882:129–131

Franke, J. and G. Menz, 2007. Multi-temporal wheat disease detection by multi-spectral remote sensing. *Precis. Agric.*, 8:161–172

Gamon, J.A., J. Peñuelas and C.B. Field, 1992. A narrow-waveband spectral index that tracks diurnal changes in photosynthetic efficiency. *Remote Sens. Environ*.,41: 35–44

Hoffer, R.M., 1978. Biological and physical considerations in applying computer-aided analysis techniques toremote sensor data. *In*: Swain, P.H.and S.M. Davis (eds.),*Towards the Remote Sensing: The Quantitative Approach*, pp: 227–289.McGraw-Hill, New York, USA

Huang, J.F. and A.Apan, 2006. Detection of Sclerotinia rot disease on celery using hyperspectral data and partial least squares regression. *J. Spat. Sci.*, 51: 129–142

Huang, W.J., D.W. Lamb, Z. Niu, Y.J. Zhang, L.Y. Liu and J.H. Wang, 2007. Identification of yellow rust in wheat using in-situ spectral reflectance measurements and airborne hyperspectral imaging. *Precis. Agric.*, 8:187–197

Jones, H.G., 2004. Application of the Clevers rmal imaging and infrared sensing in plant physiology and ecophysiology. *Adv. Bot. Res.*, 41: 107–163

Li, G.B., S.M.Zeng and Z.Q. Li, 1989. *Integrated Management of Wheat Pests*,1st edition.Press of Agriculture Science and Technology of China, Beijing

Lorenzen, B. and A. Jensen, 1989. Changes in leaf spectral properties induced in barley by cereal powdery mildew. *Remote Sens. Environ.*, 27: 201–209

Luo, J.H., W.J. Huang, X.H. Gu, N. Jin, L. Ma, X.Y. Song, G. Li and C.L. Wei, 2010. Monitoring stripe rust of winter wheat using PHI based on sensitive bands. *Spectrosc. Spect. Anal.*, 30: 184–187

Malthus, T.J., 1993. High resolution spectroradiometry: Spectral reflectance of field bean leaves infected by Botrytis fabae. *Remote Sens. Environ*., 45: 107–116

Mirik, M., G.J. Michels Jr., S. Kassymzhanova-Mirik, N.C. Elliott, V. Catana, D.B. Jones and R. Bowling, 2006. Using digital image analysis and spectral reflectance data to quantify damage by greenbug (Hemitera: Aphididae) in winter wheat. *Comput. Electron. Agric.*, 51: 86–98

Moshou, D., C.Bravo, J.West, S.Wahlen, A.McCartney, and H.Ramon, 2004. The automatic detection of 'yellow rust' in wheat using reflectance measurements and neural networks. *Comput. Electron. Agric.*, 44: 173–188

Moshou, D., C. Bravo, R. Oberti, J. West, L. Bodria, A. McCartney and H. Ramon, 2005. Plant disease detection based on data fusion of hyper-spectral and multi-spectral fluorescence imaging using Kohonen maps. *Real-Time Imaging*, 11: 75–83

Muhammed, H.H., 2005. Hyperspectral crop reflectance data for characterising and estimating fungal disease severity in wheat. *Biosyst. Eng.*, 91: 9–20

Nicolas, H., 2004. Using remote sensing to determine of the date of a fungicide application on winter wheat. *Crop Prot*., 23: 853–863

Nutter, F.W., 1989. Detection and measurement of plant disease gradients in peanut with a multispectral radiometer. *Phytopathology*, 79: 958–963

Parker, S.P., M.W.Shaw and D.J.Royle, 1995. The reliability of visual estimates of disease severity on cereal leaves. *Plant Pathol.*, 44: 856–864

Pu, R.L., M. Kelly, G.L. Anderson and P.Gong, 2008. Using CASI hyperspectral imagery to detect mortality and vegetation stress associated with a new hardwood forest disease. *Photogramm. Eng. Rem. S.*, 74: 65–75

Qin, Z.H. and M.H. Zhang, 2005. Detection of rice sheath blight for in-season disease management using multispectral remote sensing. *Int. J. Appl. Earth Obs.*, 7: 115–128

Reynolds, G.J., C.E. Windels, I.V. MacRae and S. Laguette, 2012. Remote sensing for assessing Rhizoctonia crown and root rot severity in sugar beet. *Plant Dis.,* 96: 497–505

Rouse, J.W., R.H. Haas, J.A. Schell and D.W. Deering,1974.*Monitoring Vegetation Systems in the Great Plains with ERTS*. The third earth resources technology satellite-1 symposium, 10-14December, 1973, Greenbelt, USA

Rumpf, T., A.K. Mahlein, U. Steiner, E.C. Oerke, H.W. Dehne and L. Plümer, 2010. Early detection and classification of plant diseases with Support Vector Machines based on hyperspectral reflectance. *Comput. Electron. Agric.*, 74: 91–99

Shao, H., J.Y.Wang and Y.Q.Xue, 1998. Key technology of pushbroom hyperspectral imager (PHI).*J. Remote Sens*., 2: 251–255

Sharp, E.L., C.R. Perry, A.L. Scharen, G.O. Boatwright, D.C. Sands, L.F. Lautenschlager, C.M. Yahyaoui and F.W. Ravet, 1985. Monitoring cereal rust development with a spectral radiometer. *Phytopathology*, 75: 936–939

Toler, R.W., B.D.Smith and J.C.Harlan, 1981. Use of aerial color infrared photography to evaluate crop disease. *Plant Dis.*, 65: 24–31

West, J.S., C. Bravo, R. Oberti, D. Lemaire, D. Moshou and H.A. McCartney, 2003. The potential of optical canopy measurement for targeted control of field crop disease. *Annu. Rev. Phytopathol.*, 41: 593–614

Zhang, B., X.H. Wang, J.G. Liu, L.F. Zhang and Q.X. Tong, 2000. Hyperspectral image processing and analysis system (HIPAS) and its applications. *Photogramm. Eng. Rem. S.*, 66: 605–609

Zhang, J.C., W.J. Huang, J.Y. Li, G.J. Yang, J.H. Luo, X.H. Gu and J.H. Wang, 2011. Development, evaluation and application of a spectral knowledge base to detect yellow rust in winter wheat. *Precis. Agric.*, 12: 716–731

Zhang, M.H., Z.H. Qin, X. Liu and S.L. Ustin, 2003. Detection of stress in tomatoes induced by late blight disease in California, USA, using hyperspectral remotesensing. *Int. J. Appl. Earth Obs.*, 7: 115–128

(Received 12 June 2012; Accepted 16 July 2012)